

# Josephson Vortex Qubit: Design, Preparation and Read-Out

A. KEMP<sup>1</sup>), A. WALLRAFF, and A. V. USTINOV

*Physikalisches Institut III, Friedrich-Alexander Universität Erlangen-Nürnberg,  
Erwin-Rommel Str. 1, 91058 Erlangen, Germany*

(Received July 29, 2002; accepted August 7, 2002)

PACS: 74.50.+r; 85.25.Cp

The design of a qubit based on a single Josephson vortex trapped in a shaped long Josephson junction is discussed in detail. The vortex potential is formed due to its interaction with an in-plane magnetic field and a bias current applied to the junction. The profile of the potential is calculated using a standard perturbation approach. We examine the dependence of the potential properties on the junction shape and its electrical parameters and discuss the requirements for observing quantum effects in this system. We have developed and experimentally tested methods for the preparation and read-out of vortex states of this qubit in the classical regime.

**1. Introduction** In the past years several types of different superconducting circuits [1–6] based on small Josephson junctions in the phase or charge regime have been shown to achieve parameters which are favorable for quantum computation. In Ref. [7], a qubit based on the motion of a Josephson vortex in a long Josephson junction was proposed. A major difference from the small Josephson junction qubit proposals where the effective potential is created by the Josephson or charging energy, is that in the vortex qubit the potential is formed by the magnetic interaction of the vortex magnetic moment with an external magnetic field, as described in Ref. [8].

In heart-shaped annular junctions two classically stable vortex states can be arranged, corresponding to two minima of the potential. While the external field is always applied in the plane of the long junction, its angle  $\Theta$  and strength  $h$  can be varied. The bias current across the junction can be used to tilt the potential. These parameters allow to manipulate and control the potential and to read out the qubit state using a zero-voltage critical current measurement. The scheme of readout and preparation of the state for this type of qubit was already demonstrated in the classical regime as briefly described in Ref. [9].

This paper describes details of the calculations necessary to determine the parameter range for the quantum regime, as well as details on the calculation of the effective potential for the vortex. An explanation of the implementation of the elementary single-bit quantum gates using the two in-plane magnetic field components is given. For the calculation of the potential a single-vortex perturbation theory approach [10] is used. Tunneling rates in the quantum regime are determined by numerical diagonalization of the Hamiltonian and compared to a WKB calculation.

**2. Principle of the Vortex Qubit** Josephson junctions, which have a length significantly larger and a width  $w$  smaller than the Josephson penetration depth  $\lambda_J$  are called long junctions. These junctions are described by the phase difference  $\varphi(q)$  of the two superconductors as the continuous degree of freedom along the spatial coordinate  $q$  (nor-

---

<sup>1</sup>) Corresponding author; e-mail: kemp@physik.uni-erlangen.de

malized to  $\lambda_J$ ), where  $0 < q < l$ , and  $l$  is the length of the junction (normalized to  $\lambda_J$ ). A magnetic field threading the junction corresponds to a gradient in the phase difference along the junction. An electrical field across the junction corresponds to a time derivative of  $\varphi$ . The dynamics of a long Josephson junction is governed by the perturbed sine-Gordon equation, which is discussed below.

Our experiments deal with long annular junctions. These consist of two stacked superconducting rings separated by a tunnel barrier. Since the flux in every ring is quantized, it is possible to realize a situation, in which the difference between the fluxes in two rings is one flux quantum  $\Phi_0$ . In this case a vortex of supercurrent carrying this flux quantum is formed along the junction. A resting vortex confines the magnetic flux to a characteristic size of  $\lambda_J$ . Since a moving vortex corresponds to moving magnetic flux, a voltage proportional to the speed of the vortex appears across the junction and can be detected. The capacitive energy proportional to the voltage is stored in the system. It corresponds to the kinetic energy of a moving particle. It is therefore possible to consider a vortex as a quasiparticle moving in one dimension.

The junction can be biased by a current across it. A Lorentz-type driving force is exerted by the bias current on the vortex. The vortex magnetic moment also interacts with the external field by a magnetic dipole interaction. This yields a possibility to create a potential for the vortex. The magnetic moment is always directed normal to the junction. By varying the angle of the junction centerline it is possible to change the potential energy of the vortex as it moves along the junction.

Using a geometry, which is shown in Fig. 1, it is possible to generate a double-well potential for a vortex in the junction. We chose a shape, which consists of a semi-circle of radius  $R$ , and two connected arcs, which intersect each other at an angle of  $2\beta$ . An external magnetic field  $h$  is applied, at an angle  $\Theta$ . The field can be described by the components  $h_x = h \sin \Theta$  and  $h_y = h \cos \Theta$ .

Assuming the vortex to carry a point-like magnetic moment, its stable positions of minimal magnetic energy can be easily found to be the regions, where the junction is aligned perpendicular to the field. In reality, the vortex is distributed over a length on the order of  $\lambda_J$ . This changes the potential shape considerably, and may even change its qualitative features. In the case of the double-well potential in the heart-shaped junction it may cause the barrier, which separates the two minima, to vanish.

The aim of this paper is to derive the exact effective potential in order to determine the range of parameters and geometries suitable for experiments in the thermal and quantum regime. We show that the effective potential for a vortex inside a shaped junction

is a sum of three terms, which depend on the external bias current, and the two in-plane field components. These are the three parameters which can be controlled during the experiment in order to realize degenerate bistable vortex states, change the barrier between them, lift the degeneracy in a controlled way, and, fi-

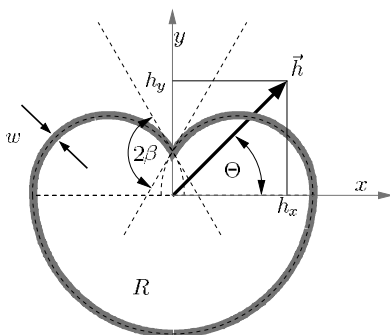


Fig. 1. Geometry of the heart-shaped junction, defined by the two geometrical parameters  $\beta$  and  $R$

nally, read-out the state using a critical current measurement. Based on this approach we proceed to quantum mechanical calculations and the calculation of the depinning current.

**3. Long Josephson Junction Model** Classically, the evolution of the phase difference  $\varphi$  between the wave functions of the two superconducting electrodes forming a long Josephson junction is described by the sine-Gordon equation

$$\sin(\varphi) = \varphi_{qq} - \varphi_{tt}, \quad (1)$$

where the temporal coordinate is denoted by  $t$ , normalized to the plasma frequency  $\omega_p^{-1}$ , discussed below. Subscripts denote partial derivatives.

Adding the terms for the inductive energy, the capacitive energy and the Josephson energy yields the corresponding Hamiltonian

$$H = \int_0^l \left( \frac{1}{2} \varphi_q^2 + \frac{1}{2} \varphi_t^2 + 1 - \cos \varphi \right) dq \quad (2)$$

with the characteristic energy scale  $E_0$ , discussed below. The temporal derivative  $\varphi_t$  corresponds to the normalized voltage across the junction, the spatial derivative  $\varphi_q$  corresponds to the normalized magnetic field in the junction.

Single-vortex solutions of Eq. (1) in a non relativistic approximation for infinitely long junctions are given by

$$\varphi(q, q_0)^{\text{vortex}} = \pm 4 \arctan(\exp(q - q_0 - vt)), \quad (3)$$

where  $q_0$  denotes the vortex center of mass and  $v$  its velocity normalized to the Swihart velocity  $\bar{c}$ , which is the characteristic velocity for the electromagnetic waves in the junction.

In the case of weak magnetic field and small bias current, the interaction with field and current can be modeled using perturbation theory. In Ref. [10], a bias current  $\gamma$  (normalized to the critical current) was found to exert a driving force of  $2\pi\gamma$  on the vortex. The influence of the external magnetic field on a shaped junction was studied theoretically [8] and experimentally [11] for a circular shape of the annular junction. The sine-Gordon equation was discussed previously for annular junctions of small ( $2\pi r < \lambda_J$ ) and large radius ( $2\pi r > \lambda_J$ ) in [12]. We use the overlap geometry, which is known to generate very little self field of the bias current. In [13] we determined experimentally the self-field effect for circular geometries corresponding to the heart-shaped junctions by measuring the dependence of the critical current on the angle of the external magnetic field. Since during the operation of the qubit no current is flowing, we made no attempt to treat the self-field quantitatively. Before we further investigate the more complex junction shapes, we need to define the characteristic scales and normalizations.

**4. Scales and Constants** In a long Josephson junction there are three important scales, which characterize the classical and quantum dynamics of the unperturbed system.

The Josephson length

$$\lambda_J = \frac{\Phi_0}{2\pi} \sqrt{\frac{1}{L^* e_J}} \quad (4)$$

is determined by the inductance  $L^*$  and the Josephson coupling energy  $e_J$  per unit length in the junction. The distance  $\lambda_J$  is the characteristic lateral dimension of a resting Josephson vortex. The Josephson coupling energy is related to the critical current density  $j_c$  as  $e_J = w j_c \Phi_0 / 2\pi$ , where  $w$  denotes the width of the long Josephson junction.

Small amplitude linear wave solutions of the phase are described by a dispersion relation. At the wave number  $k = 0$  (a homogeneous oscillation over the whole junction) the corresponding frequency is the so-called Josephson plasma frequency  $\omega_p$ , given by

$$\omega_p = \frac{2\pi}{\Phi_0} \sqrt{\frac{e_J}{C^*}}, \tag{5}$$

where  $C^*$  denotes the capacitance of the junction per unit length. The temporal coordinate of Eq. (1) is normalized by  $\omega_p^{-1}$ . The product  $\lambda_J \omega_p = \bar{c}$  is the Swihart velocity.

All energies are normalized to the characteristic energy

$$E_0 = \frac{\Phi_0}{2\pi} \sqrt{\frac{e_J}{L^*}} = e_J \lambda_J. \tag{6}$$

The energy unit  $E_0$  is equal to the Josephson coupling energy of a small Josephson junction of the area  $\lambda_J w$ .

The rest energy of a vortex is equal to eight in units of  $E_0$ , where half the energy is stored in the Josephson coupling and the other half is stored in the inductive energy. Since the speed of light equals unity in the normalized units, the rest mass of the vortex  $m_0 = 8$ .

Applying these normalizations to the Planck's constant  $\hbar$ , which has the unit of action, yields a normalized Planck's constant  $\hbar_{\text{norm}}$ , given by

$$\hbar_{\text{norm}} = \hbar \frac{\omega_p}{E_0} = \hbar \left( \frac{2\pi}{\Phi_0} \right) \sqrt{\frac{L^*}{C^*}}. \tag{7}$$

The normalized Planck's constant  $\hbar_{\text{norm}}$  does not depend directly on the Josephson coupling energy, but  $L^*$ ,  $C^*$  and  $e_J$  are related to each other through the barrier thickness.

**5. Perturbation Theory Approach** We apply a perturbation theory approach similar to that of Refs. [8, 10] and reduce the dynamics of the system to the center of mass motion of the vortex as with its coordinate  $q_0$  being the only degree of freedom.

In the lowest order of perturbation theory it is assumed that the phase gradient profile imposed by the external magnetic field and the phase gradient profile corresponding to a resting vortex do not influence each other, which requires that at least one of these is assumed to be small. The inductive energy term of Eq. (2) for  $\varphi_q = \varphi_q^{\text{vortex}} + \varphi_q^{\text{ext}}$  yields

$$U^{\text{ext}}(q_0) = \int_0^l \frac{1}{2} [\varphi_q^{\text{vortex}}(q - q_0) + \varphi_q^{\text{ext}}(q)]^2 dq. \tag{8}$$

Expanding Eq. (8) yields

$$U^{\text{ext}}(q_0) = \int_0^l \frac{1}{2} \varphi_q^{\text{vortex}}(q - q_0)^2 dq + \int_0^l \frac{1}{2} \varphi_q^{\text{ext}}(q)^2 dq + \int_0^l \varphi_q^{\text{vortex}}(q - q_0) \varphi_q^{\text{ext}}(q) dq. \tag{9}$$

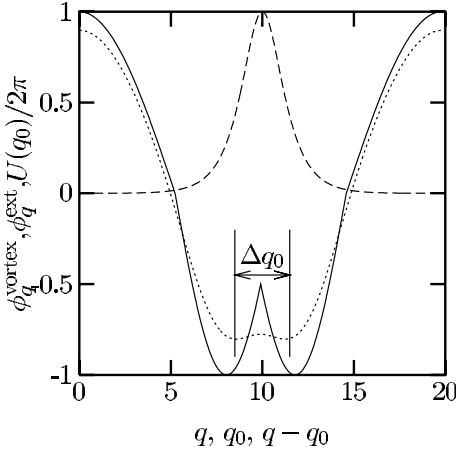


Fig. 2. Phase gradient (solid line)  $\varphi_q^{\text{ext}}(q)$  introduced by the external magnetic field, the phase gradient (long dashed)  $\varphi_q^{\text{vortex}}(q - q_0)$  associated with phase profile of a vortex (shifted to  $q - q_0 + 10$  for visibility), and the effective potential (short dashed)  $U(q_0)$ , given by Eq. (8) with  $\gamma = 0$

Since we are only interested in the dependence of  $U^{\text{ext}}(q_0)$  on  $q_0$ , we can neglect the first two constant terms which are the magnetic energy of a resting vortex and the energy of the external magnetic field in the junction, respectively. The last term, which is a convolution of the externally introduced phase gradient with the phase gradient profile of the vortex, is the potential energy corresponding to the magnetic dipole interaction.

The influence of the bias current  $\gamma$  can be taken into account by adding a potential term corresponding to a constant driving force. This yields the total potential

$$U(q_0) = \varphi_q^{\text{vortex}}(q - q_0) *_q \varphi_q^{\text{ext}}(q) - \gamma 2\pi q_0 \quad (10)$$

for the vortex, where  $*_q$  denotes the convolution in  $q$ . The effect of the convolution of the externally introduced phase gradient with the magnetic profile of the vortex is indicated in Fig. 2. The phase gradient (solid line) is induced by a field in  $y$ -direction ( $\Theta = \pi/2$ ), see heart shaped junction depicted in Fig. 1. While the derivative of the phase gradient is discontinuous at  $q = l/2$ , the resulting potential is smooth at this point. Furthermore, the distance  $\Delta q_0$  between the minima and the height  $U_0$  of the barrier are diminished by the convolution. In general, all local perturbations are smoothed to a length of the order of  $\lambda_J$ .

**6. Effective Potential in Shaped Junctions** We will now discuss how a specific geometry, like that of Fig. 1, is related to the potential profile for an arbitrary field angle  $\Theta$ .

The phase difference gradients correspond to shielding currents, which flow in the superconducting electrodes of the junction. Since these shielding currents are orthogonal to the magnetic field, the phase gradient along the junction is proportional to the scalar product of the normal vector of the junction with the external magnetic field. This is equivalent to the physical interpretation of the vortex magnetic moment interacting with the external magnetic field. Expanding the scalar product to its (orthogonal) components

$$\varphi_q^{\text{ext}}(q) = \mathbf{n}(q) \cdot \mathbf{h} = n_x(q) h_x + n_y(q) h_y \quad (11)$$

yields an equation, in which the phase gradient is linear in each component of the field. Since also the convolution of the vortex magnetic moment with the external magnetic field is a linear operation, it is possible to separate the convolution for the calculation

of the potential into two components,

$$\begin{aligned} & \varphi_q^{\text{vortex}}(q - q_0) *_q \varphi_q^{\text{ext}} \\ & = \varphi_q^{\text{vortex}}(q - q_0) *_q n_x(q) h_x + \varphi_q^{\text{vortex}}(q - q_0) *_q n_y(q) h_y. \end{aligned} \tag{12}$$

We now abbreviate  $\varphi_q^{\text{vortex}}(q - q_0) *_q n_x(q)$  by  $U_x$ , and substitute Eq. (12) into Eq. (10). This yields

$$U(q_0) = U_x(q_0)h_x + U_y(q_0)h_y - \gamma 2\pi q_0 \tag{13}$$

as the total potential for the vortex motion.

We now return to the geometry in Fig. 1. From the symmetry of the heart it can be seen immediately, that  $\mathbf{n}_y(q)$  is symmetric with respect to  $q = 0$  and  $q = l/2$ , while  $\mathbf{n}_x(q)$  is antisymmetric with respect to these points. Therefore, also  $U_y(q_0)$  and  $U_x(q_0)$  are symmetric and antisymmetric, respectively.  $U_y(q_0)$  and  $U_x(q_0)$  are depicted in Fig. 3 for the junction in Fig. 1, having the normalized length  $l = 20$ .

Of special interest is the region at  $q = l/2$ , since  $U_y$  forms a double-well potential there, if the radius  $R$  is large enough in relation to the Josephson length. The influence of a change in the Josephson length on the double-well potential is shown in Fig. 4, where for a heart of the same radius effective potentials are shown using different Josephson lengths. The distance between the wells and the height of the barrier are strongly diminished with increasing Josephson length. At a certain critical value of the Josephson length the barrier ceases to exist for this geometry.

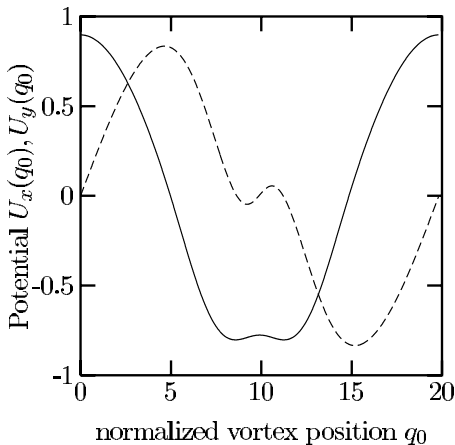
**7. Quantum Mechanics of a Vortex** The Schrödinger equation for the center of mass motion of a vortex is given in normalized units by

$$-i\hbar_{\text{norm}} \Psi = \hat{H} \Psi = (\hat{T} + \hat{U}) \Psi, \tag{14}$$

where  $\hat{U}$  denotes the potential energy operator, and

$$\hat{T} = \frac{\partial}{\partial q^2} \frac{\hbar_{\text{norm}}^2}{16} \tag{15}$$

corresponds to the kinetic energy operator for a particle of mass  $m_0 = 8$ . A numerical discretization and diagonalization of  $\hat{H}$  yields the eigenstates, which are shown in Fig. 5 for  $w = 0.3 \mu\text{m}$ ,  $R = 50 \mu\text{m}$ ,  $j_c = 1000 \text{ A/m}^2$ .



The tunnel splitting between the two lowest energy eigenstates is proportional to the expected tunneling rate. The numerically calculated values for the tunnel splitting are shown as points in Fig. 6 and tunneling rates calculated in WKB ap-

Fig. 3. The potential for horizontally ( $\theta = 0^\circ$ ) and vertically ( $\theta = 90^\circ$ ) applied magnetic field

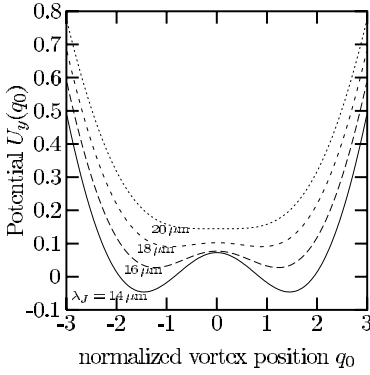


Fig. 4

Fig. 4. Potential for a single junction, in dependence of the vortex position  $q_0$ , with different curves for different  $\lambda_J$

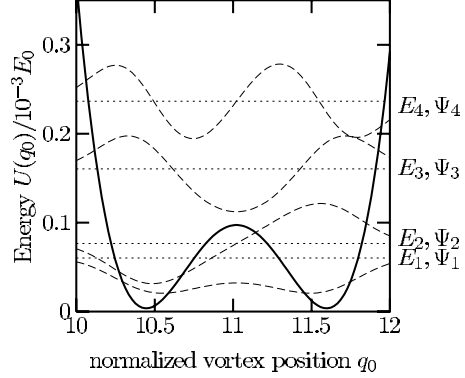


Fig. 5

Fig. 5. Calculated lowest energy eigenstates for a junction of  $w = 0.3 \mu\text{m}$ . The energy levels are indicated by the dotted lines, the wave functions are indicated by the dashed lines

proximation are shown by the solid line. It can be seen, that the tunneling rate can be tuned within the experimentally accessible field-range by four orders of magnitude.

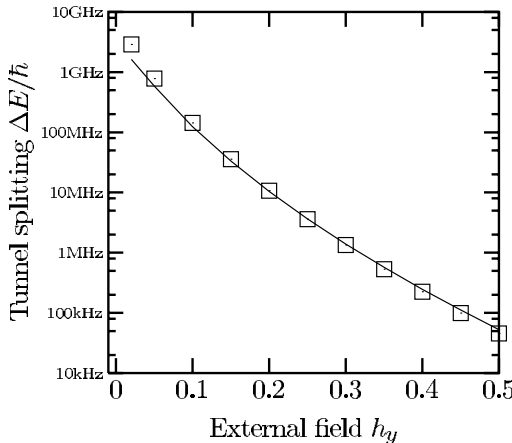
Applying a small  $x$ -component breaks the degeneracy of the potential, since an antisymmetric potential component will be added. If this component is small, perturbation theory yields a correction for the energy eigenvalues of the uncoupled states inside each well,

$$\Delta U = \langle \Psi | \hat{U}_x | \Psi \rangle h_x. \quad (16)$$

Since  $U_x(q_0) = -U_x(-q_0)$ , and the states localized in the left/right well are symmetric, one state is shifted up, while the other state is shifted down in energy.

At low temperatures, the vortex dynamics in the double-well potential is reduced to that of a two-state system, the Hamiltonian of which can be written as

$$H = \Delta E(h_y) \sigma_x + \Delta U \sigma_z, \quad (17)$$



where  $\Delta E$  is the overlap of the ground states, found by the WKB-method. It must be noted, that  $\Delta E(h_y)$  depends exponentially on  $h_y$  while  $\Delta U$  depends only linearly on  $h_x$ . By controlling  $h_x$  and  $h_y$  it is possible to realize all single qubit operations.

Fig. 6. Tunnel splitting between the states, according to the energy splitting of the lowest energy eigenstates

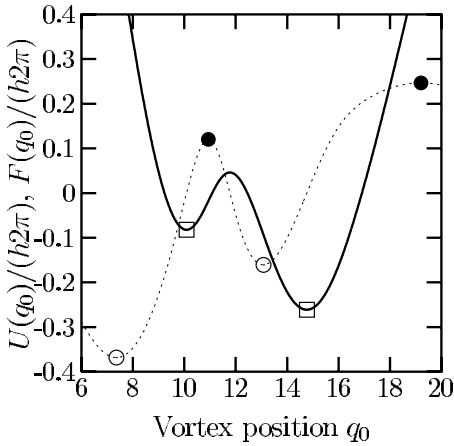


Fig. 7. Minima of the potential  $U(q_0)$  (solid line) are marked by open squares. The minima of the pinning force (dotted line) are marked by open circles, the maxima by solid circles

**8. Readout and Depinning Current** For the experimental test of the readout procedure in the classical regime [9], we are interested in the depinning current of the vortex which is an experimentally accessible parameter. A vortex starts to move, when the pinning force due to the external field is compensated by the force exerted by the bias current. Calculating the deriva-

tive of Eq. (10) yields

$$F(q_0) = \frac{\partial U(q_0)}{\partial q_0} = \frac{\partial U_x(q_0)}{\partial q_0} h_x + \frac{\partial U_y(q_0)}{\partial q_0} h_y - \gamma 2\pi \tag{18}$$

for the force  $F(q_0)$  acting on the vortex. The equilibrium positions correspond to a zero net force. Using Eq. (13), we can write a condition for the equilibrium positions as

$$F_x(q_0) (h_x/h) + F_y(q_0) (h_y/h) = (\gamma/h) 2\pi, \tag{19}$$

where  $F_x$  denotes  $\partial U_x(q_0)/\partial q_0$ .

Solutions of Eq. (19) vanish, if local maxima/minima in the force are exceeded by  $\gamma 2\pi$ . A vortex trapped in one of these stable equilibrium positions will be depinned at these currents. The corresponding current is therefore called the depinning current  $\gamma_{\text{dep},i}$ , where  $i$  is the index, if several stable positions exist. In Fig. 7, a potential without bias current is shown, together with the corresponding force. Each minimum of the potential, indicated by an open square, has one corresponding minimum (open circle) and maximum (solid circle) of the force. For a given angle  $\Theta$  of the external field,  $(h_x/h)$  and  $(h_y/h)$  in Eq. (19) are constant. Therefore, the ratio  $\rho_{\text{dep},i} = (\gamma_{\text{dep},i}/h)$  is constant for a specific angle of the field.

The dependence of  $\rho_{\text{dep},i}$  on the angle of the external magnetic field can be found numerically. In Fig. 9, the dependence of  $\rho_{\text{dep},i}$  on the field angle  $\Theta$  is plotted by two lines for  $i = 1$  and  $i = 2$ . We performed a test, if the vortex would be trapped in the remaining stable positions. This happens if the spatial distance between the depinning position and the next maximum in the potential is so small, that the vortex does not gain enough kinetic energy to overcome this maximum. In such a case, the vortex will get retrapped at the remaining stable position. If the current is increased, the vortex is depinned from this remaining position at the corresponding depinning current. In this case we plotted the latter value of the depinning current in Fig. 9.

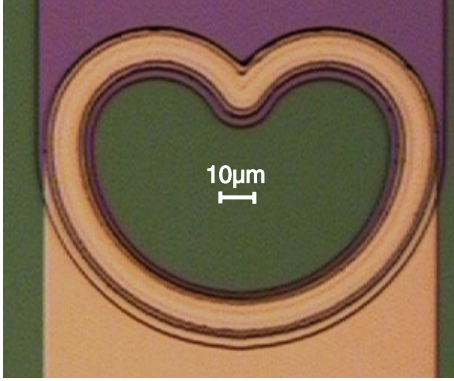


Fig. 8 (online colour). Optical microscope picture of the junction used for the experimental test. Parameters are  $R = 50 \mu\text{m}$ ,  $\beta = 60^\circ$ ,  $w = 3 \mu\text{m}$ ,  $j_c = 796 \text{ A/cm}^2$

**9. Experimental Test** We carried out an experimental test of the preparation and readout scheme proposed above using the junction shown in Fig. 8.

Figure 9 shows the measured depinning current in dependence on the angle  $\Theta$  of the external magnetic field. We measured the depinning current of the vortex after a clockwise and counterclockwise rotation as described in Ref. [9]. The two directions of rotation correspond to circles and squares in Fig. 9, respectively.

From the dependence of the depinning current on the angle the two ways of preparation can be associated with the numerically determined values of  $\rho_{\text{dep},i}$ . At  $\Theta = 270^\circ$ , we find numerically that  $\rho_{\text{dep},1} = \rho_{\text{dep},2}$ . This angle corresponds to an antisymmetric potential, which has a symmetric first derivative. Therefore, the maximum values of the pinning force are identical. In Fig. 9 this theoretically predicted crossing is found in the experiment. The pinning for state (2) is slightly higher than expected. This small discrepancy of  $\rho_{\text{dep},i}$  indicates additional pinning possibly due to inhomogeneities, residual flux or geometrical reasons.

In the experiment, only at the readout angle  $\Theta \approx 330^\circ$  the crossover between retrapping in state (2) and depinning from state (1) is observed as numerically predicted. The crossover from retrapping in state (1) to detection of state (2) shows a large discrepancy to the numerical prediction. We attribute the difference between the experimental and the numerical data in Fig. 9 in the range  $\Theta \approx 45^\circ$  to  $260^\circ$  to the damping which has been neglected in the numerical calculation.

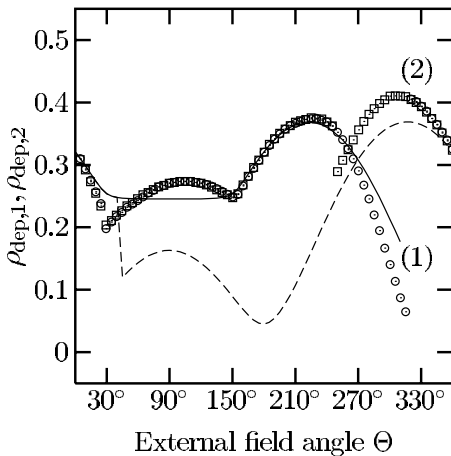


Fig. 9. Normalized depinning current  $\gamma_{\text{dep}}/h$  plotted versus the angle  $\Theta$  of the external field. Lines correspond to numerical calculation, squares (clockwise preparation of state,  $i = 1$ ) and circles (counterclockwise preparation of state,  $i = 2$ ) are the experimentally measured values

**10. Conclusions** We demonstrated a preparation and readout scheme for the vortex qubit in the classical regime and thus verified the existence of bistable states. The obtained experimental results agree well with the numerical calculations. Small discrepancy is most probably due to the specific geometry of junction electrodes, which may cause additional pinning (see Ref. [14]). Another source of it is the neglect of damping in the numerical calculation.

Using the tools developed, further experimental steps as statistical measurements of vortex states in the thermal or quantum regime can be performed. Numerical and WKB calculations show that in sub-micron-width junctions with a low damping one should be able to observe quantum effects. For the operation of the vortex qubit it is necessary to control the width and height of the barrier. While the height can be controlled in a wide range by the magnetic field, the distance of the stable minima is determined during fabrication of the sample, by the Josephson length and the junction geometry.

The macroscopic quantum coherence experiment using a vortex in a long narrow junction requires production of narrow junctions of well-defined geometry with a precise control of the critical current density. Thermal activation measurements can examine, if corrections to the one-dimensional model of the junction are required. By going to low temperatures, the crossover to the quantum tunneling regime is expected. In this regime, it should be possible to probe the tunnel splitting by applying microwaves, which would also allow to determine the quality factor of the system.

**Acknowledgements** We wish to thank D-Wave Systems and the DFG for funding this work and the IPHT Jena for sample fabrication.

## References

- [1] Y. NAKAMURA, YU. A. PASHKIN, and J. S. TSAI, *Nature* **398**, 786 (1999).
- [2] J. R. FRIEDMAN, VIJAY PATEL, W. CHEN, S. K. TOLPYGO, and J. E. LUKENS, *Nature* **406**, 43 (2000).
- [3] CASPAR H. VAN DER WAL, A. C. J. TER HAAR, F. K. WILHELM, R. N. SCHOUTEN, C. J. P. M. HARMANS, T. P. ORLANDO, SETH LLOYD, and J. E. MOOIJ, *Science* **290**, 773 (2000).
- [4] J. M. MARTINIS, S. NAM, J. AUMENTADO, and C. URBINA, *Phys. Rev. Lett.*
- [5] D. VION, A. AASSIME, A. COTTET, P. JOYEZ, H. POTHIER, C. URBINA, D. ESTEVE, and M. H. DEVORET, *Science* **296**, 889 (2002).
- [6] Y. YU, S. HAN, X. CHU, S. CHU, and Z. WANG, *Science* **296**, 889 (2002).
- [7] A. WALLRAFF, YU. KOVAL, M. LEVITCHEV, M. V. FISTUL, and A. V. USTINOV, *J. Low Temp. Phys.* **118**, 543 (2000).
- [8] N. GRØNBECH-JENSEN, P. S. LOMDAHL, and M. R. SAMUELSEN, *Phys. Lett. A* **154**, 14 (1991).
- [9] A. KEMP, A. WALLRAFF, and A. V. USTINOV, *Physica C* **368**, 324 (2002).
- [10] D. W. McLAUGHLIN and A. C. SCOTT, *Phys. Rev. A* **18**, 1652 (1978).
- [11] A. V. USTINOV, B. A. MALOMED, and N. THYSSEN, *Phys. Lett. A* **233**, 239 (1997).
- [12] N. MARTUCCIello and R. MONACO, *Phys. Rev. B* **54**, 9050 (1996).
- [13] A. KEMP, Fluxon States in Heart-Shaped Josephson Junctions, Master's thesis, Physikalisches Institut III, Universität Erlangen-Nürnberg, 2001; [http://www.pi3.physik.uni-erlangen.de/ustinov/publications/thesis/dipl\\_kemp.pdf](http://www.pi3.physik.uni-erlangen.de/ustinov/publications/thesis/dipl_kemp.pdf).
- [14] D. MÜNTER, T. DODERER, H. PRESSLER, S. KEIL, and R. P. HUEBENER, *Phys. Rev. B* **58**, 14518 (1998).